BAND GAP DETERMINATION OF CHEMICALLY DEPOSITED LEAD SULPHIDE BASED HETEROJUNCTION THIN FILMS

C. AUGUSTINE[a,b*], M. N. NNABUCHI[a]
[a]*Department of Industrial Physics, Ebonyi State University, Abakaliki, Nigeria*
[b]*Department of Physics/Geology/Geophysics, Federal University Ndufu-Alike Ikwo, Nigeria*

Lead sulphide based heterojunction thin films have been synthesized via simple, inexpensive and highly reproducible chemical bath deposition technique. Apart from lead sulphide film which was deposited at room temperature, other films were deposited at 353K in an electric oven. The grown films were annealed between 273K-673K, 1 hour using electric furnance and characterized with RBS, XRD, SEM, and spectrophotometer for compositional, structural, morphological, and optical/solid properties respectively. XRD analysis reveals that the films are polycrystalline as depicted by the sharp peaks. SEM analysis show large grains with well-defined grain boundaries. There are no cracks in the surface morphologies of Mn_3O_4/PbS, CuO/PbS and NiO/PbS films, which accounted for high mechanical stability of the films. Spectrophotometric analysis indicated high absorbance for all the film samples exhibiting maximum in the UV region and minimum in the IR region. The absorbance, absorption coefficients and band gap were greatly affected by thermal annealing. In particular, the band gaps of Mn_3O_4/PbS, CuO/PbS, and PbS/NiO thin films show a decreasing trend with increasing annealing temperatures while NiO/PbS film depicts increase in band gap with increasing annealing temperatures. The band gap of Mn_3O_4/PbS decreases from 3.95eV for as-deposited to 3.80eV for annealed at 473K and 3.70eV at 673K. The band gap of CuO/PbS decreases in the range 4.00eV-3.75eV. PbS/NiO has band gap decreases from 1.70eV for as-deposited to 1.50eV for annealed at 473K and 1.25eV for annealed at 673K. The band gap of NiO/PbS increased from 1.38eV for as-deposited to 1.63eV for annealed at 473K and 2.38eV for annealed at 673K. Based on the exhibited properties of the films, it can be concluded that they are promising materials for selective coatings for solar cells, effective coatings for poultry houses and fabrication of optoelectronic devices etc.

(Received August 23, 2017; Accepted September 29, 2017)

Keywords: XRD, SEM, band gap, temperature, thin film

1. Introduction

In the quest for an alternative energy source due to environmental pollution, global warming and increase in energy demand, solar energy which is a renewable energy has been considered as an alternative [1]. The solar energy production is made possible by using a solar cell. A solar cell is a device that converts sun light energy to electricity via Photoelectric effect [2]. Silicon based solar cell tend to occupy the solar energy market, but thin film solar cell is currently gaining recognition due to its low cost in comparison to the high cost of silicon based solar cell which has made the entire production of solar energy to be expensive [3].

An important class of thin film compounds are the chalcogenides and metal oxides, which are important materials with many applications in industries. Chalcogenides such as PbS is widely reported for its myriads of applications. For instance, Lead sulphide (PbS) is an important direct narrow gap semiconductor material with an approximate energy band gap of 0.4 eV at 300K and a relatively large excitation Bohr radius of 18 nm [4]. It has been widely studied because of its applications in infrared detection [5], photography [6], Pb^{2+} ion selective sensors [7], solar absorption [8] and thin film solar cells [9]. The absorption edge has been found to be red shifted as

* Corresponding Author: emmyaustine2003@yahoo.com

the particle size increased [10]. Practical applications of thin oxide films are in homes, electronics, recording heads, memory, and microwave devices. Most oxide thin films can also be applied in highly reproducible gas and humidity sensor materials [11]. Oxides thin film materials have been one of the most attractive research topics in Physics and Material Science. Materials like Fe_2O_3, CrO_2, manganese pervoskites, double and layered pervoskites, $BiFeO_3$, and more recently, transition metal oxide thin films such as NiO, CuO, Mn_3O_4 to mention but a few have been reported and have received new and exciting attentions [12]. For instance, nickel oxide (NiO) is an attractive material because of its chemical stability as well as structural, optical, electrical and magnetic properties. Nickel oxides have been used in different applications like positive electrode in batteries [13], fuel cell [14], solar thermal absorber [15], gas sensors [16], photodetectors [17] and electrochromic devices [18-20]. NiO thin films have useful applications as optically active counter electrodes for window materials and the optical quality of NiO film is improved by annealing [21]. Also, Copper oxide (CuO) thin films could be employed in solar cells, photo sensor applications, photothermal application, high temperature superconducting materials [22-24]. Copper oxide based sensors have applications in the fabrication of gas sensing devices because of the conductivity changes induced by the reaction of gases with surface absorbed oxygen [25, 26]. Manganese oxide thin films have been shown to have applications in various fields, such as optoelectronic devices, secondary batteries, supercapacitors, ion exchange, catalysis and oxidation process [27-30].

Currently, there is considerable interest in the deposition of core-shell thin film material, due to the potential of tailoring both the lattice parameters and the band gap by controlling depositions parameters [31, 32]. In 2012, the photovoltaic applications of ZnO/PbS quantum dot was reported [33]. In the same year, [34] studied the thermal properties of TiO_2/PbS nanoparticle solar cells. In 2103, the fabrication of ZnO/CuO core-shell nanoarrays for inorganic-organic heterojunction solar cells was reported [35]. [36], prepared MnS/ZnS and PbS/ZnS core-shell nanostructures in 2014. In the same year, [37], fabricated ternary stack thin films of CdS/PbS and PbS/CdS on plane glass substrates at room temperature. In 2015, deposited Sn-Al core-shell nanocomposites as thin film anode for lithium-ion batteries, the growth of TiO_2/CuO nanofibers for enhanced solar hydrogen generation and the effect of thermal annealing on TiO_2/CuO core-shell thin film were reported [38-40]. In 2016, [41], studied the particle size analysis for different substrates of ZnS/ZnO thin film. [42], deposited ZnO-CdS core-shell composite nanorods in 2016. Recently, in 2017, the growth of Ti_3C_2/TiO_2/CuO ternary nanocomposites, fabricated Ge/Si core-shell quantum dots in alumina were reported [43, 44]. We contribute by reporting the structural, morphological and optical properties of Mn_3O_4-PbS, CuO-PbS, NiO-PbS and PbS-NiO core-shell thin films.

2. Materials and Methods

2.1 Materials

Many materials were used in this work for the deposition, annealing grown parametric variations and characterization of Manganese oxide/lead sulphide (Mn_3O_4/PbS), Copper oxide/lead sulphide (CuO/PbS), Nickel oxide/lead sulphide (NiO/PbS), and Lead sulphide/nickel oxide (PbS/NiO) thin films. Apart from the routine laboratory equipments such as beakers, reagents, measuring cylinders, syringes, bottles, thermometers, time piece and conical flasks etc., other relatively more specialized materials as discussed were employed.

2.1.1 Equipments for Deposition

Commercially purchased microscopic glass slides were used as substrates. A laboratory electric oven (Gallen Kamp model INA305) of 0^oC-80^oC was used to maintain desired constant temperature for the deposition all the films except PbS film which was deposited at room temperature. Laboratory Oven (model No. DHG-9101.SA) of temperature range 0^oC-250^oC and electric furnance of 0^oC -1000^oC were used for annealing the grown films. Magnetic stirrer with hot plate (Model EC 1010) was used for stirring and heating where necessary. A digital weighing

balance (Adventurer Pro model AV313) was used for the determination of masses. The p^H of growth solution baths was measured with a MAC digital p^H metre (MSW-552 model).

2.1.2 List of Chemicals

The following chemicals were commercially purchased and used for the film deposition. Lead nitrate, sodium hydroxide, thiourea, nickel sulphate, ammonia of analytical grade, cadmium sulphate, manganese chloride, ammonium chloride, copper sulphate, potassium chloride and hydrochloric acid.

3.2 Methods

3.2.1 Preparation of Substrate

The microscopic glass slides used as substrates prior to deposition were soaked in concentrated hydrochloric acid for 24 hours, removed and washed with foam-sponge in ethanol and finally rinsed in distilled water. Thereafter, they were then drip dried in air. Thereafter the substrates were rinsed in distilled water and drip dried in air. The degreased, cleaned surface has the advantage of providing nucleation centers for the growth of the films, hence, yielding highly adhesive and uniformly deposited films.

3.2.2 General Deposition Procedure

The solution growth of thin films of Mn_3O_4/PbS, CuO/PbS, NiO/PbS and PbS/NiO in this work involved measuring with syringes desired volumes of definite molar solutions of the required chemicals for a particular precursor compound specified in the relevant sections into growth baths (50-100ml beakers) to form the growth mixture. The growth mixtures were topped with specific volume of distilled water and stirred with magnetic stirrer. Pre-cleaned glass substrates were then inserted vertically into the growth mixtures using synthetic foam. Synthetic rubber foam was used as cover to the reaction bath to protect it from dust particles and other environmental impurities as well as to suspend the substrate into open bath. This arrangement did not allow for an airtight reaction bath. This will prevent condensation on the inner surface of the cover. The set-up were each placed in the chamber of an oven set at the desired constant temperatures for specified periods. The coated substrates were removed at the end of the specified periods, rinsed with distilled water and hung with clips in open air to dry. The loaded substrates were labelled for identification.

3.2.3 Annealing Procedure

The deposited films were annealed in an electric oven and furnance between 200^{o}C and 400^{o}C temperature range. To begin annealing, the oven and furnance were opened and the loaded slide quickly placed on the substrate holder inside it with clean pair of tongs and the oven closed, with the time noted. At the end of the desired annealing period, the oven was opened and the loaded substrate again quickly brought out, using the pair of tongs. The film on the substrate was then allowed to acquire room temperature. The purpose of annealing is to know the temperature at which the samples can be exposed to without damage and also to investigate the effect of temperature on the properties of the films. One sample served as the control during characterization.

3.2.4 Synthesis of Mn_3O_4/PbS Thin Film

The chemical bath for the deposition of Mn_3O_4 was made up of a mixture of 12mls of 1M $MnCl_4$, 12mls of 1M NH_4Cl, 12mls of 10M NH_3 and 24mls of water. Five (5) clean glass slides were then inserted vertically into the solution. The deposition was allowed to proceed at temperature of 80^{o}C for 5 hours after which the coated substrates were removed, washed with distilled water and allowed to dry. The deposited Mn_3O_4 was inserted in a mixture containing 5mls of 0.2M $Pb(NO_3)_2$, 5mls of 1M SC $(NH_2)_2$, 5mls of 1M NaoH and 35mls of distilled water put in that order in 100ml cleaned and dried beaker for 50 minutes to form Mn_3O_4/PbS core-shell thin film. Four of the deposited films were annealed in an oven at various temperatures (200^{o}C and 400^{o}C) for 1hr. One of the samples was left un-annealed to serve as the control during characterization. The same procedure was repeated for growing the other thin films.

3.2.5 Synthesis of CuO/PbS Thin Film

The chemical bath for the deposition of CuO was made up of a mixture of 4mls of 1M $CuSO_4$, 4mls of 1M KCl, 2mls of 10M NH_3 and 13mls of distilled water. The deposition took place at 80^oC bath temperature for 3 hours. To deposit CuO/PbS film, the deposited CuO was inserted into a mixture containing 5mls of 0.2M $Pb(NO_3)_2$, 5mls of 1M SC $(NH_2)_2$, 5mls of 1M NaoH and 35mls of distilled water put in that order in 50ml beaker for 50 minutes.

3.2.6 Synthesis of NiO/PbS Thin Film

First, NiO film was deposited with chemical bath containing10mls of 1M $NiSO_4$, 5mls of 10M NH_3 and 27mls of distilled water into 50ml beaker with a P^H value of 10.The deposition was allowed to proceed at temperature of 80^oC for 1 hour. The deposition of NiO/PbS was accomplished by inserting the already deposited NiO film into a mixture containing 5mls 0.2M $Pb(NO_3)_2$, 5mls of 1M SC $(NH_2)_2$, 5mls of 1M NaoH and 35mls of distilled water put in that order in 50ml beaker for 50 minutes.

3.2.7 Synthesis PbS/NiO Thin Film

First, PbS film was deposited with a chemical bath made of 5mls of 0.2M $Pb(NO_3)_2$, 5mls of 1M SC $(NH_2)_2$, 5mls of 1M NaoH and 35mls of distilled water put in that order in 50ml cleaned and dried beaker. The deposition took place at room temperature for 50 minutes. To obtain the PbS/NiO core-shell, the PbS already formed (core) was inserted in a mixture containing 10mls of 0.2M-1M $NiSO_4$, 5mls of 10M NH_3 and 27mls of distilled water into 50ml beaker. Deposition was allowed to proceed at temperature of 353K for 1 hr.

3.2.8. Characterization of the deposited core-shell thin films

Rutherford backscattering (RBS) was used to determine the elemental compositions, depth profile and thicknesses of the films by Proton Induced X-ray Emission (PIXE) scans on the samples from a Tandem Accelerator Model 55DH 1.7MV Pellaton. The elemental compositions and the thickness of the film samples were determined from the plots of normalized yield against channels and energy generated through RBS spectrometer. The spectrometer which has inbuilt sensor processor used the simulated input data analysis to generate the graphs and determine the elements contained, the thickness of the sample and the relative concentrations of each sample. The crystal structure and phase analysis of the deposited films were carried out at room temperature with an X-ray diffractrometer Rigaku Ultima IV model, using gracing incident at 30 mA, 40KV with CuKα radiation of wavelength λ=0.15406nm selected by a diffracted beam monochromator. The thin films were scanned continuously between 0 to 90^o at a step size of 0.034 and at a time per step of 56.7s. The XRD diffractograms of intensity versus 2θ values were generated and displayed. Phase identification was then made from an analysis of intensity of peaks versus 2θ, using ICDD data. Origin graphing analysis software was used to plot the intensity versus 2θ. Thermo scientific GENESYS 10S model UV-VIS spectrophotometer was used to determine the absorbance of the deposited films in the wavelength range of 300-1000 nm. The absorbance (A) of the film was directly digitally read. The Transmittance (T), Reflectance (R), and optical/solid state properties were estimated from the absorbance spectra. With the aid of the computer origin graphing software, graphs of optical dependent parameters versus wavelength and photon energy were plotted. The optical bang gaps of the samples were determined from the absorption spectra by simply extrapolating the linear portion of the plot of absorption coefficient squared against photon energy to photon energy axis. The intercept on photon energy axis gives the band gap energy. Scanning Electron Micrscope (Tescan model) was used to observe the morphology of the deposited core-shell thin films.

3. Results and discussion

3.1 XRD Analysis

Typical XRD diffractograms of Mn_3O_4/PbS, CuO/PbS, NiO/PbS, and PbS/NiO thin films are presented in figures 1(a), (b), (c), and (d) respectively. From fig. 1(a), the peaks at 2θ values of 25.964^o, 30.075^0, 43.059^0 and 50.978 are attributed to galena PbS (JCPDS 00-005-0592). These were assigned to the diffraction line produced by (111), (200), (220) and (311) planes. The peaks at angles of 18.000^o, 32.316^o, 36.450^o and 50.710^o are identified to be hausmannite Mn_3O_4 (JCPDS 00-024-0734) and are assigned diffraction lines produced by (101), (103), (202) and (105) planes respectively. However, additional peaks of 28.082^o, 29.615^o and 30.645^o are identified to be Pb_2MnO_4 (JCPDS 00-036-0844) phase and assigned diffraction lines produced by (131), (330) and (231) planes. The existence of this high pressure magnetic phase implies that the film can be used in magnetic memory device and spintronics because of quantum dot effect. From fig.1 (b), the prominent peak at 2θ value of 35.583^o corresponding to (212) planes is attributed to copper hydroxide sulphate phase which is in good agreement with Joint Committee on Powder Diffraction Standard (JCPDS) data cards (JCPDS 00-011-0653). One of the most important aspect revealed from fig. 1(b), is the growth of anglesite lead oxide sulphate phase $PbSO_4$ (JCPDS 00-036-1461) at 2θ values of 29.680^o and 44.546^o corresponding to (121) and (231) reflections. Fig. 1(c) depicts prominent peaks among them are peaks at 2θ values of around 25.964^0, 30.075^{0}corresponding to diffraction lines produced by (111), (200) planes respectively which are attributed to galena PbS (JCPDS 00-005-0592), 33.065^o and 38.542^o corresponding to diffraction lines produced by (100) and (101) planes of theophrastite $Ni(OH)_2$ (JCPDS 00-014-0117) phase. From fig. 1(d), the peaks at 2θ values of 25.964^o, 30.075^0, 43.059^0 and 50.978 are attributed to galena PbS (JCPDS 00-005-0592). These were assigned to the diffraction line produced by (111), (200), (220) and (311) planes. However, the additional peaks at angles of 37.249^o, 43.276^o, 62.879^o and 75.416^o are identified to be NiO (JCPDS 00–047-1049) and are assigned diffraction line produced by (111), (200), (220) and (311) planes of the bunsenite phase.

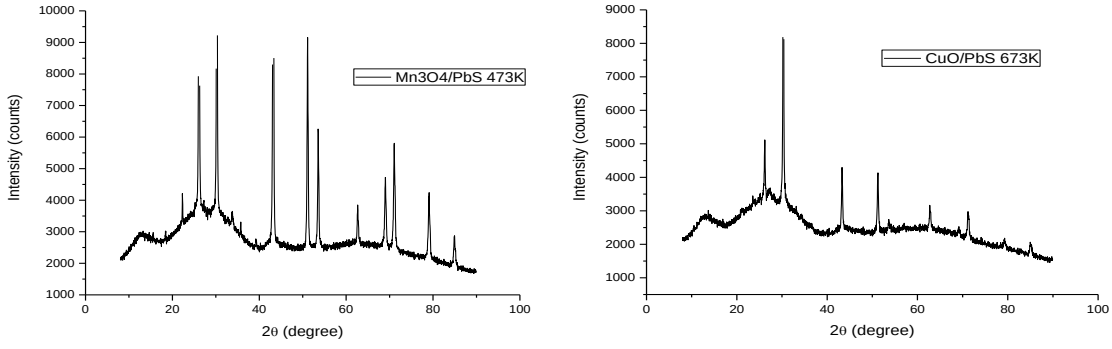

a) b)

Fig. 1(a): XRD diffractogram of Mn_3O_4/PbS thin film
(b): XRD diffractogram of CuO/PbS thin film

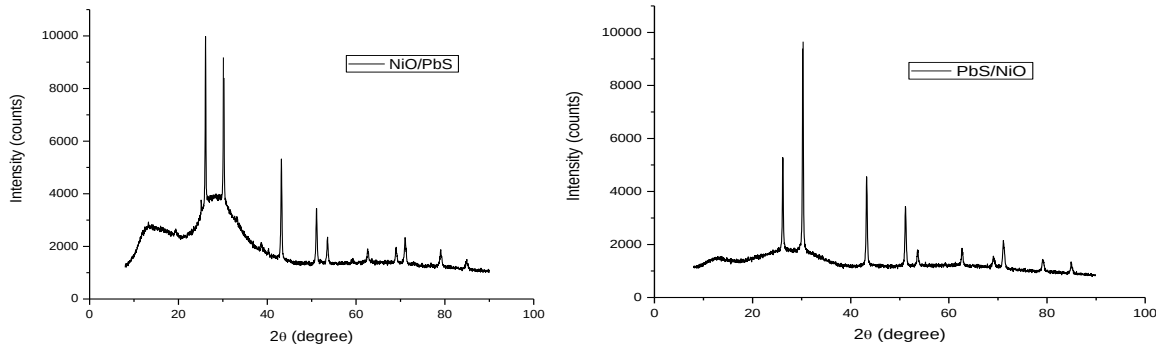

Fig. 1(c): XRD diffractogram of NiO/PbS thin film
(d): XRD diffractogram of PbS/NiO thin film

3.2. Morphological Analysis

Fig. 2a, 2b, 2c and 2d depicts the SEM images of Mn_3O_4/PbS, CuO/PbS and NiO/PbS, PbS/NiO thin films. Generally, the morphologies of all the film samples are characterized by large grains and well surface coverage with well-defined grain boundaries. Engagement of small grains of the films in flower–like structure is clearly observed in SEM image of CuO/PbS thin films, suggesting nanostructured films. The observed long network of structure ordering makes the CuO/PbS film good material for design of light-trapping configuration for solar cells [45]. The absence of cracks in the SEM images of the film samples accounts for the high mechanical stability of the deposited films.

.

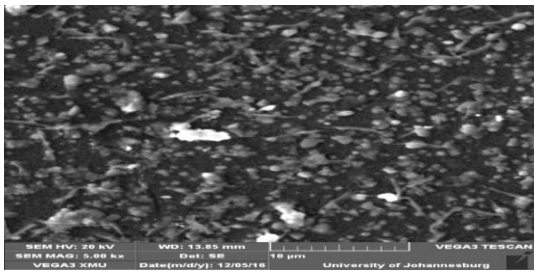

Fig. 2a: SEM images of Mn_3O_4-PbS core-shell thin film

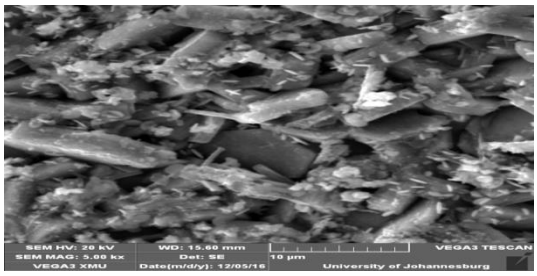

Fig. 2b: SEM image of CuO/PbS core-shell thin film

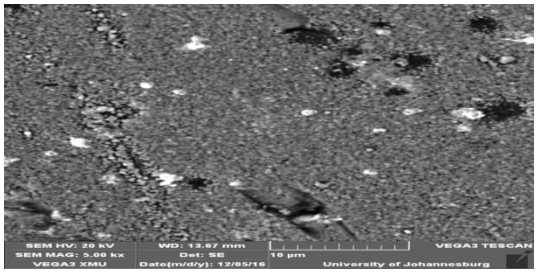

Fig. 2c: SEM image of NiO/PbS core-shell thin film

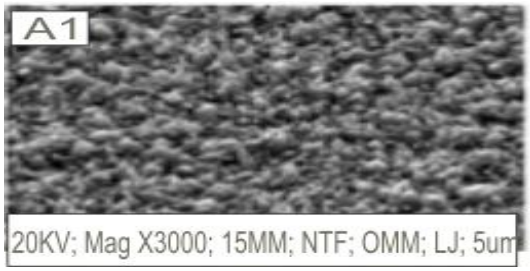

Fig. 2d: SEM image of PbS/NiO core-shell thin film

3.3 Rutherford Backscattering (RBS) Analysis

The RBS analysis was done to determine the elemental compositions and thicknesses of Mn_3O_4/PbS, CuO/PbS, NiO/PbS and PbS/NiO core-shell thin films. Figs. 3a, 3b, 3c and 3d, depicts the RBS micrographs of Mn_3O_4/PbS, CuO/PbS, NiO/PbS and PbS/NiO core-shell thin films respectively. In RBS analysis, film thickness is determined by the width of the peak. The concentration is determined by the intensity or height of the peak. Table 1 depicts the thickness of the four categories of films. From table 1, it is clearly seen that thermal annealing has profound effect on the thickness of the films. Thickness of film is a very important parameter. Apart being used to classify films into thick or thin, the thickness of films influences the properties. The percentage compositions of the deposited films as well as glass slide as deciphered by RBS analysis are Mn_3O_4/PbS: 70.63% Pb, 17.78% Mn, 29.33% S and 82.22% O; CuO/PbS: 0.59% Pb, 5.64% Cu, 33.16% S and 94.36% O; NiO/PbS: 22.44% Pb, 65.32% Ni, 12.25% S and 71.24% O; PbS/NiO: 8.11% Pb, 1.10% Ni, 2.78% S and 95.55% O; Glass slide: 0.30% Fe, 6.00% Ca, 3.50% K, 34.00% Si, 5.20% Al, 25% Na and 26.00%.

Table 1: Summary of thickness of the film samples in nanometer (nm)

Sample	As-deposited	473K	673K
Mn_3O_4/PbS	1026	1084	1540
CuO/PbS	650	482	470
NiO/PbS	416	492	713
PbS/NiO	694	565	503

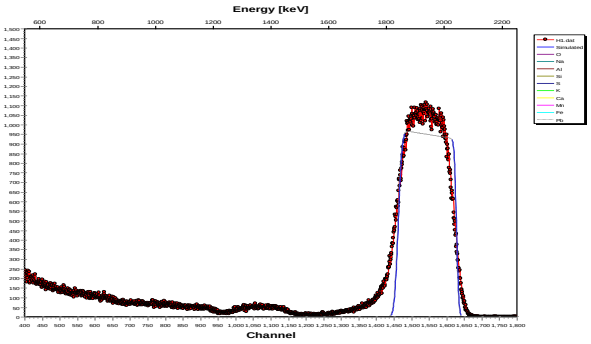

Fig. 3a: RBS micrograph of Mn_3O_4-PbS thin film

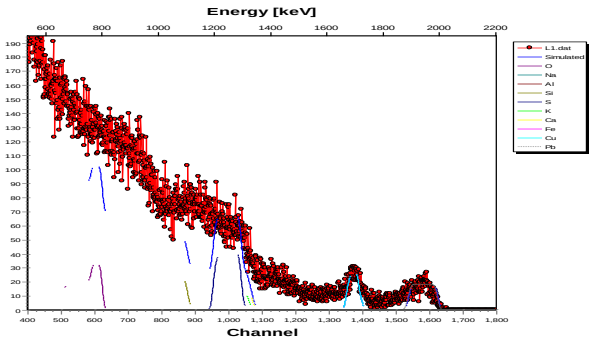

Fig. 3b: RBS micrograph of CuO-PbS thin film

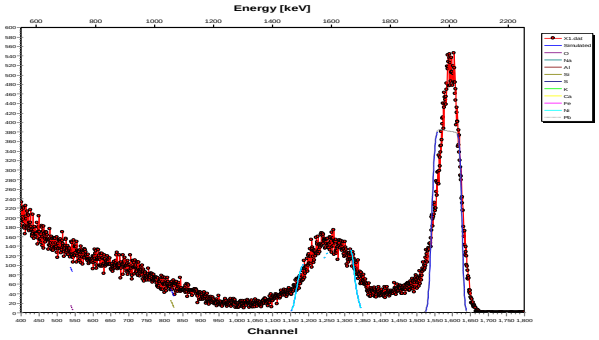

Fig. 3c: RBS micrograph of NiO-PbS thin film

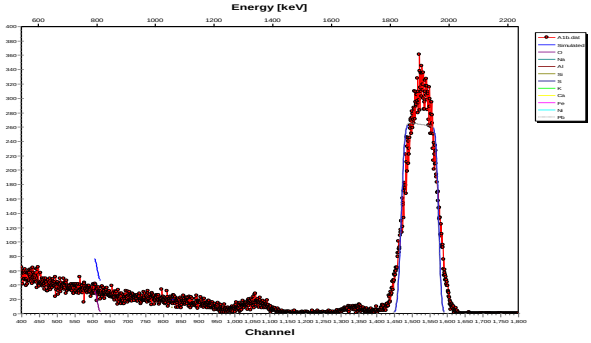

Fig. 3d: RBS micrograph of PbS/NiO thin film

3.4 Optical properties

The effects of annealing temperatures on the optical and solid state properties of the films were investigated. It is clearly seen that thermal annealing has profound effects on the absorbance, absorption coefficient and band gap of the four categories of films. Fig. 4a, 4b, 4c and 4d depicts the plots of absorbance against wavelength of Mn_3O_4/PbS, CuO/PbS, NiO/PbS and PbS/NiO thin films respectively. All film samples exhibit maximum absorbance in the UV region and minimum in the infrared region. The heated layers absorb better than the as-deposited layers for all film samples except for NiO/PbS film where a reversed trend was observed. The results indicates that thermal annealing has profound effect on the absorbance. This is attributed to the re-organization of the grains at various annealing temperatures. Studies have shown that the schottky barrier can be removed by annealing and the improvement in material quality and the increase of the effective surface area due to the porous nature introduced by heat treatment [46].

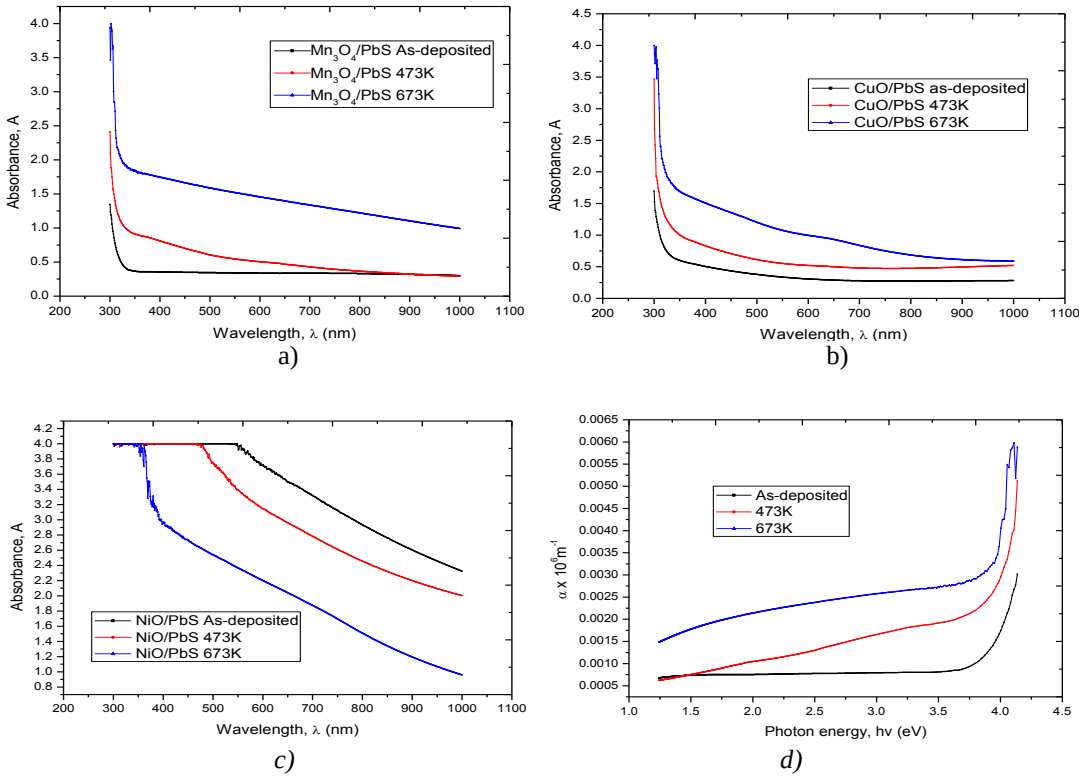

Fig. 4a: Absorbance spectra as deposited and annealed at 473K and 673K for a) Mn_3O_4-PbS; b) CuO-PbS; c) NiO-PbS ; d) of PbS-NiO

The plot of absorption coefficient versus photon energy for the thin films under review namely Mn_3O_4/PbS, CuO/PbS, NiO/PbS and PbS/NiO, are shown in Fig. 5a, 5b, 5c and 5d respectively. The film samples generally have high absorption coefficient exhibiting a maximum for the heated layers except for NiO/PbS film where the reverse is the case. The increase in absorption coefficient with annealing temperature could be attributed to the distribution of the grains at various annealing temperatures. The concentration of carriers has also been reported to affect the absorption coefficient of thin films. Increase in temperature increases the carrier concentration and mobility of the charge carriers and this affects the absorption coefficient [47].

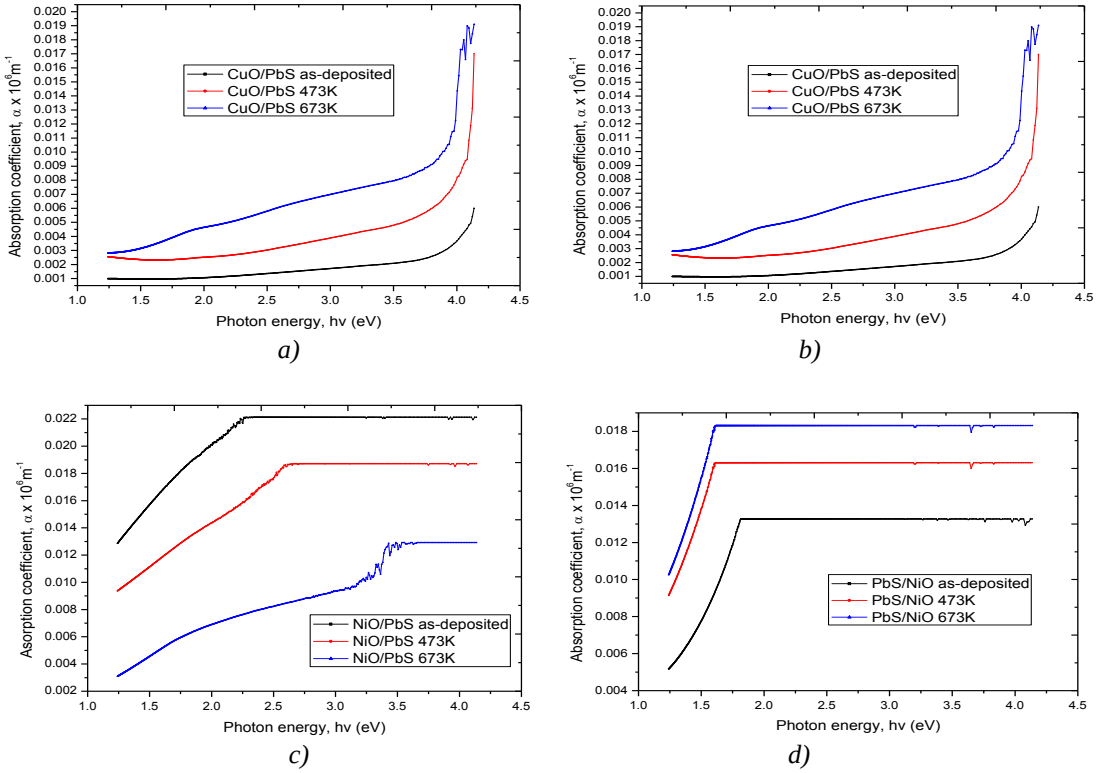

Fig.5c: Plots of absorption coefficient versus photon energy of core-shell thin film
a) Mn_3O_4/PbS; b) CuO/PbS ; c) NiO/PbS; d) PbS/NiO

The absorption coefficient was calculated using already established relation [4]

$$\alpha = \frac{2.3026A}{t} \tag{1}$$

Where α is the absorption coefficient, A is absorbance and t is the thickness of the film.

Figs. 6a, 6b, 6c and 6d displayed the plots of $(\alpha h\upsilon)^2$ against hυ for Mn_3O_4/PbS, CuO/PbS, NiO/PbS and PbS/NiO respectively. Table 2 depicts the summary of band gap of the four categories of films. The result shows that the band gaps were affected largely by annealing temperature. The film samples show decreasing trend of band gap with increase in annealing temperature except for NiO/PbS film which exhibited a reverse trend. The band gap decreases could be due to many body effects like the exchange energy due to electron-electron and electron-impurity interactions which occurs when the carrier density exceeds a certain value and causes narrowing (red shift) of the band gap energy [48]. The decrease of the band gap can also be related to quantum confinement effect which has two consequences: First it splits the conduction band into discrete levels and secondly, it reduces the density of states available in the conduction band such that at 673K, the carrier concentration gets to its critical value leading to the collapse of the potential barrier at the grain boundaries and hence abrupt decrease in the band gap at 673K [49]. This is consistent with the results of [50], who reported decrease in band gap of TiO_2/ZnO at different annealing temperatures. In our previous work, the band gap decreases with annealing temperatures of PbS/NiO/CdO heterojunction thin film was reported [51]. [52], reported decrease in band gap of ZnSe as a result of increase in annealing temperatures. [53], attributed such decrease in the band gap of the heated layers to the increase in grain size or related phenomena, caused by the annealing effects. This decrease in band gap as result of increasing annealing temperatures is collaborated by the fact that the band gap can be expressed in terms of the effective mass approximation as [54]

$$\Delta E_g = \frac{\frac{\hbar^2\pi^2}{2R^2}\left(\frac{1}{M_e}+\frac{1}{M_h}\right)-\left(1.786e^2\right)}{\varepsilon R} \quad (2)$$

Where M_e and M_h are the effective masses of the electrons in the conduction band and of holes in the valance band respectively, and ε is the static dielectric constant of the material and ΔE_g is the change in band gap of the semiconductor materials. The first term in the above equation represents the particle in-a-box quantum localizations energy and has simple $1/R^2$ dependence, where R is the particle radius. The second term represents the Coloumb energy with 1/R dependence. Therefore, as R increase due to the increase in the crystallite size associated with high temperature annealing, the value of ΔE_g will decrease. Processes like annealing which increases the particle size decreases the band gap and occurs in most cases with post deposition annealing [46]. Also as temperature increases, the band gap decreases because the crystal lattice expands and the interatomic bonds are weakened. On the other hand, the increase in band gap of NiO/PbS with annealing temperatures could be attributed to the Burstein-Moss shift which occurs when the electron carrier concentration exceeds the conduction band edge density of states [55]. The increase in band gap as a result of increase in annealing temperatures has been reported by other authors. [56], reported band gap increase with annealing temperatures of TiO_2/Fe_2O_3 thin film, [57], reported increase in band gap of NiSe and CuSe thin films with increasing annealing temperatures. The large band gap possessed by Mn_3O_4/PbS and CuO/PbS thin films implies that the films can be used for applications where electrical isolation is required such as cooling blankets for nuclear reactors. The band gap of the films were calculated using Tauc's relation [58]:

$$(\alpha h\nu)^n = A\left(h\nu - E_g\right) \quad (3)$$

Where A is band edge parameter and value of n determines the nature of optical transition (n = ½ indicates direct transition and n = 2 indicates indirect transition). Linearity of the dependence indicates direct transitions. Extrapolating the linear regions to αhν = 0 gives the value of band gap.

Table 2: Summary of band gap of the deposited film samples in electron volt (eV)

Sample	*As-deposited*	*473K*	*673K*
Mn_3O_4/PbS	*3.95*	*3.80*	*3.70*
CuO/PbS	*4.00*	*3.88*	*3.75*
NiO/PbS	*1.38*	*1.63*	*2.38*
PbS/NiO	*1.70*	*1.50*	*1.25*

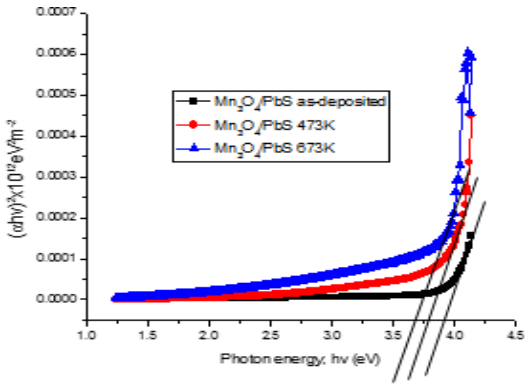

Fig.6a: Plots of $(\alpha h\nu)^2$ versus $h\nu$ of Mn_3O_4/PbS core-shell thin film

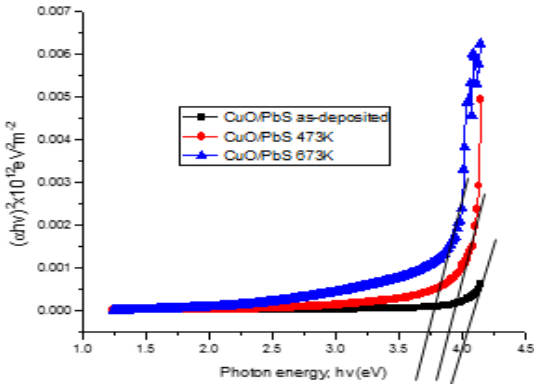

Fig.6b: Plots of $(\alpha h\nu)^2$ *versus* $h\nu$ *of CuO/PbS core-shell thin*

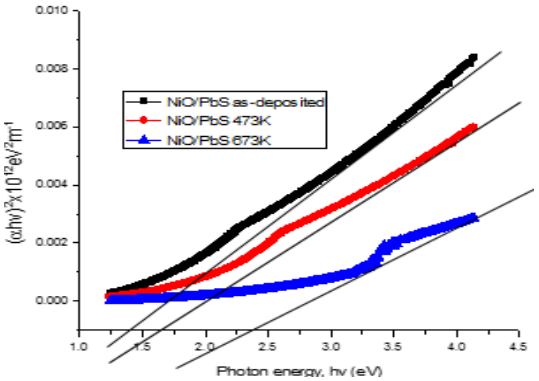

Fig.6c: Plots of $(\alpha h\nu)^2$ *versus* $h\nu$ *of NiO/PbS core-shell thin*

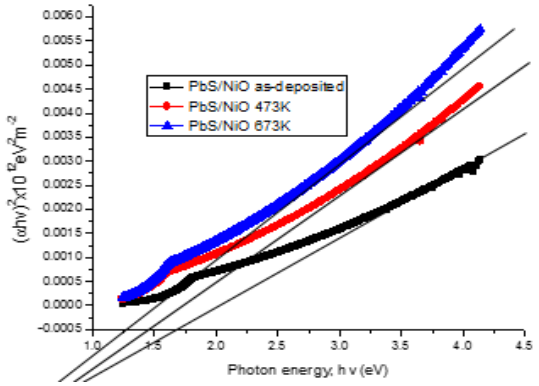

Fig.6d: Plots of $(\alpha h\nu)^2$ *versus* $h\nu$ *of PbS/NiO core-shell thin*

4. Conclusions

Chemical Bath Deposition process has been employed for deposition of lead sulphide based thin films through post deposition annealing. The compositional, microstructural, optical/solid state properties of the as-deposited and thermally annealed lead sulphide based thin films show strong dependence on the deposition parameters. The spectral analyses revealed that thermal annealing have profound effect on the optical and solid state properties of the deposited

thin films. In general, this research has showcased in a quantitative manner, compositional, structural, optical and solid state essential for potential solar cells fabrication, optoelectronic, architectural materials etc.

References

[1] M. M. Aliyu, R. S. Shehu, Photovoltaic Solar cells-New materials and Technology, Electrical Electronic Engineering Conference proceeding, Kaduna Polytechnic, 97-107 (2011).
[2] B. L. Theraja, Textbook of Electrical Technology; S.C. Hard and Company Ltd, 243 – 2434 (2007).
[3] T. Minami, Semiconductor Science and Technology, **20** (4), 535-544 (2005).
[4] J. P. Mahashabde, A. M. Patil, K. E. Suryavanshi, S. N. Patil, International Journal of Advanced Scientific and Technical Research, **3**(4), 731(2014).
[5] P. Gadenne, Y. Yagil, G. Deutscher, J. Appl. Phys., **66**, 3019 (1989).
[6] P. K. Nair, M. T. S. Nair, Sol. Ener. Mater. **15**, 431(1987).
[7] H. K. Hirata, B. Higashiyama, Chem. Soc. Jpn. **44**, 2420 (1971).
[8] T. K. Chaudhuri, S. Chattersjes. S Proceedings of the international conferences on thermoelectronics, **11**, 40 (1992).
[9] J. Hernández-Borja, Y. V. Vorobiev, R. Ramírez, Sol. Energy Mater. Sol. Cells **95**, 1882 (2011).
[10] N. Choudhary, B. K. Sharma, Indian J. Pure. Appl. Phy. **46**, 261 (2008).
[11] J. L. Gunjakar, A. M. More, K. V. Gurav, Applied Surface Science, **254**, 5844 (2008).
[12] R. P. Borges, P. Ferreira, A. Srsiva, R. Gohclaves, M. Rosa, A. P. Goncalves, R. Sihvada, M. J. V. Laurence, F. J. V. Santos, M. Godinho, Physical B, **404**,1398 (2009).
[13] C. M. Lambert, G. Nazri, P. C. Yu, Sol. Energy Matter. **16**, 1 (1987).
[14] N. Shaigan, D. G. Ivey, W. Chen, Journal of .Electrochem Soc. **156** (6), B765 (2009).
[15] K. R. Cerc, P. Bukovec, B. Pihlar, V. A. Surea, B. B. Orel, G. Drazie, Solid State Ionics **165**, 191 (2003).
[16] I. Hotovy, J. Huran, L. Spiess, R. Capkovic, S. Hascik, Vacuum **58**(2-3), 300 (2000).
[17] M. C. Leong, I. M. Seongil, Applied Surface Science, **244** (1-4), 435 (2005).
[18] F. F. Ferreira, M. H. Tabacniks, M. C. A. Fantini, I. C. Faria, A. Gorenstein, Solid State Ionics. **86**, 971 (1996).
[19] K. K. Purushothaman, G. Muralidharan, Journal of Sol-Gel Science Technology **46**, 190 (2008).
[20] C.M. Lambert, G. Nazri, P.C. Yu, Sol. Energy Matter. **16**, 1 (1987).
[21] P. Vikas, P. Shailesh, C. Manik, G. Prasad, S. Ratnakar, S. Shashwat, J. Pradeep, Journal of Surface Engineered Materials and Advanced Technology **1**, 35 (2011).
[22] B. Balamurugan, B. R. Mehta, Thin Solid Films **396**, 90 (2001).
[23] J. Zhou, X. Wu, G. Teeter, B. To, Y. Yan, R.G. Dhere, T. A. Gessert, , Phys. Stat. Sol **241** (3), 775 (2004).
[24] L. B. Chen, N. Lu, C. M. Xu, H. C. Yu, T. H. Wang, Electrochim Acta, **54**, 4198 (2009).
[25] S. Saito, M. Miyayama, K. Koumoto, H. Yanagida, Journal of American Ceramics Society, **68**, 40 (1985).
[26] E. Traversa, Journal of Intelligent Material System Structure, **6**, 860 (1995).
[27] S. E. Fendorf, R. J. Zasoski, Environ. Sci. Technol., **26** (1), 79 (1992).
[28] Y. Chabre, J. Pannetier, Progress in Solid State Chemistry **23**, 1 (1995).
[29] X. K. Huang, H. J. Yue, A. Attia, Y. J. Yang, Journal of Electrochemical Society **154** (1), 26 (2006).
[30] P. U. Asogwa, Journal of Optoelectronics and Biomedical Materials **2**(3), 109 (2010).
[31] B. R. Sankagal, C. D. Lokhande, Materials Chemistry and Physics **14**, 126 (2002).
[32] D. Rakesh, K. Doshi, M. Satish, S. K. Agarwal, H. K. Sehgal, Thin solid films **80**, 447 (2002).
[33] C. Ariana, ZnO/PbS quantum dot heterojunction photovoltaics, M.Sc Thesis, Universitat De Barcelona, pp. 3-11(2012).

[34] P. Derek, Z. Guangmei, J. B. Alison, Z. Daoli, B. A. Glenn, A. C. Sue, Nanomaterials and Nanotechnology, **2**, 1 (2012).
[35] L. Zhifeng, H. Jianhua, H. Li, G. Keying, L. Yajun, C. Ting,W. Bo, L. Xiaoping, Materials Chemistry and Physics, **141**, 804 (2013).
[36] M. D. Priya, V. Shally, S. J. Geradin, S. D. Mowy, Journal of Applied Physics **6**(4), 01 (2014).
[37] A. I. Onyia, M. N. Nnabuchi, Study of Optical properties of CdS/PbS and PbS/CdS Heterojunction Thin Films Deposited using Solution Growth Technique, Proceedings of the 1st African International Conferences/Workshop on Applications of Nanotechnology to Energy, Health and Environment, UNN, March 23-29, (2014).
[38] L. Wei, K. Zhang, Z. Tao, J. Chen, Journal of Alloys and composites **644**, 742 (2015).
[39] Z. Liangliang, H. Minghui, W. H. Ghim, Nano Energy **11**, 28 (2015).
[40] D. U. Onah, E. I. Ugwu, J. E. Ekpe, American Journal of Nano Research and Applications, **3**(3), 62 (2015).
[41] M. Kavitha, M. Saroja, V. K. Romesh, G. Jenifer, International Journal of Thin Films Science and Technology **5**(2), 137 (2016).
[42] M. Kavitha, M. Saroja, V. K. Romesh, G. Jenifer, International Journal of Thin Films Science and Technology **5**(2), 137 (2016).
[43] L. Yang, Y. Meihuan, Z. Aiguo, H. Qianku, W. Libo, , Journal of Nanomaterials, 1-5 (2017).
[44] N. Nikolina, S. P. Jordi, B. R. Ivancica, G. Jorg, H. Rene, B. Sigrid, I. Mile, B. Maja, Ge/Si core-shell quantum dots in alumina: tuning the optical absorption by the core and shell size, nanophotonics, 1-8 (2017).
[45] T. Soga, Fundamentals of Solar cell Nanostructured Materials for Solar Energy Conversion UK, Elsevier, 3-4 (2006).
[46] J. D. Dipalae, S. Shaeed, F. Siddiqui, R. Ghosh, R. Birajdar, A. Ghule, R. Sharma, Advance in Applied Science Research, **2**(4), 471 (2011).
[47] A. L. Cai, J. F. Muth, Mat. Res. Soc. Symp. Proc **764**,120 (2003).
[48] N. Sharma, R. Kumar, Advances in Applied Science Research **5**(2), 111 (2014).
[49] T. O. Daniel, Effect of substrate temperature on zinc oxide doped aluminium. M.Sc Desertation, Federal University of Technology, Minna, Niger State (2015).
[50] P. E. Agbo, M. N. Nnabuchi, Chalcogenide Letters **8**(4), 273 (2011).
[51] C. Augustine, M.N. Nnabuchi, Band gap Determination of Novel PbS-NiO-CdO Heterojunction thin film for possible Solar Energy Applications, *Journal of Ovonic Research*, **13**(4), 233-240 (2017).
[52] A. R. Chikwenze, A. J. Ekpunobi, Optical Journal of Science, Engineering and Technology. **14** (2), 7495 (2007).
[53] P. A. Nwofe, P. E. Agbo, Journal of Non-Oxide Glasses **9** (1), 9 (2017).
[54] Z. Jing, T. Xia, P. Yuan, F. Xiao, J. Zeng, Applied Surface Science **257**, 393 (2010).
[55] Z. Biju, H. Wen, Journal of semiconductor processing **34**(5), 2 (2013).
[56] P. E. Agbo, M. N. Nnabuchi, D. U. Onah, Journal of Ovonic Research **7**(2), 29 (2011).
[57] A. R. Chikwenze, Solution growth and characterization binary selenide thin films for device applications, Ph.D Thesis, Department of Industrial Industrial Physics, Ebonyi State University, Abakaliki, 305-338 (2012).
[58] C. D. Lokhande, B.R. Sankapal, R.S. Mane, H.M. Pathan, M. Muller, M. Giersig, V. Ganesan, Appl. Surf. Sci. **193**, 1 (2002).